

Path to collapse for an isolated Néel skyrmion

S. Rohart,^{*} J. Miltat, and A. Thiaville*Laboratoire de Physique des Solides, CNRS, Univ. Paris-Sud, Université Paris-Saclay, 91405 Orsay Cedex, France*

(Received 6 January 2016; revised manuscript received 20 May 2016; published 14 June 2016)

A path method is implemented in order to precisely and generally describe the collapse of isolated skyrmions in a Co/Pt(111) monolayer, on the basis of atomic scale simulations. Two collapse mechanisms with different energy barriers are found. The most obvious path, featuring a homogeneous shrinking, gives the largest energy, whereas the lowest energy barrier is shown to comply with the outcome of Langevin dynamics under a destabilizing field of 0.25 T, with a lifetime of 20 ns at around 80 K. For this lowest energy barrier path, skyrmion destabilization occurs much before any topology change, suggesting that topology plays a minor role in the skyrmion stability. On the contrary, an important role appears devoted to the Dzyaloshinskii-Moriya interaction, establishing a route towards improved skyrmion stability.

DOI: [10.1103/PhysRevB.93.214412](https://doi.org/10.1103/PhysRevB.93.214412)

I. INTRODUCTION

The Dzyaloshinskii-Moriya interaction (DMI) [1,2] promotes noncollinear order, and thus is at the origin of new states of magnetism that are neither ferro- nor antiferromagnetic. They differ from structures arising from competing exchange interactions [3,4] by a chirality that is fixed. The stabilization of skyrmions [5], which correspond to whirling configurations that are topologically different from the uniform ground state, is one of its most fascinating consequences. First found in arrays which are the ground state of the system [6,7], they can also be obtained as solitons, i.e., localized excited states above the energy of the ferromagnetic ground state [8,9]. In that case, promising applications in spintronics are foreseen, such as ultradense memories [10] or logic devices [11]. Recently, significant progress has been made in the control of isolated skyrmions, including nucleation and motion under spin-polarized currents [12–14].

The stability of skyrmions is a major issue regarding their possible use in room-temperature devices. As they are distinct from the uniform state by a different topology, an exceptional stability may be expected [10]. Topology, described by the topological number S , is intimately linked to a continuous description of magnetism, in the framework of micromagnetics [15]. As integer values of S only are possible, no continuous path linking different topological states exists, hence the topological stability. In the discrete atomic description, however, topological considerations do not hold and, in particular, no univoque equivalent of S exists. On the other hand, topologically forbidden transitions in magnetism are experimentally observed, e.g., in the case of magnetic bubble collapse [16] or vortex core reversal [17,18], as well as for skyrmions [12,13]. Thus, the details of topological transitions have to be studied in order to understand how the topological paradox is lifted, and to evaluate the intrinsic stability of skyrmions. In the continuous micromagnetic description within a three-dimensional world, the topological transition is realized by the injection of a topological singularity called a Bloch point, where the continuity of magnetism is broken [15]. For skyrmions, nucleation and annihilation have been observed

in various simulations [19–24] under thermal fluctuations or spin transfer torque excitations, but a detailed mechanism is still missing to evidence the role of topology in the stability. Whereas a Bloch point cannot, strictly speaking, exist in two-dimensional samples, an equivalent process has been mentioned [19,21], but it is not clear how it relates to the intermediate configuration at the energy barrier.

In this paper, we investigate by atomic scale calculations the path linking an isolated skyrmion to the ferromagnetic state and its consequences on the skyrmion stability. Using static calculations to determine the collapse path, we describe the collapse process and show the importance of DMI in the stability. Results are further confirmed by the study of thermally induced collapse, using Langevin dynamics. Rather than using arbitrary parameters, we focus our calculations on skyrmions in a Co monolayer on Pt(111). This is one of the most promising systems that has been studied in order to control isolated skyrmions. Indeed, while it presents a large DMI [25–27], the strong out-of-plane magnetic anisotropy and Heisenberg exchange prevent intrinsic destabilization of the ferromagnetic order, which is key to enabling isolated skyrmions. In addition, we develop a very fast shortcut to minimum energy path calculations in the case where a reaction coordinate along the path is known.

II. MAGNETIC MEDIUM AND SKYRMION DESCRIPTION

The magnetic layer is described at the atomic scale, by a set of classical spins \mathbf{S}_i on a hexagonal lattice realizing an epitaxial Co monolayer on a Pt(111) substrate, with a site-to-site distance $a = 2.51 \text{ \AA}$. The energy is given by

$$E = \sum_{(i,j)} [-J \hat{\mathbf{s}}_i \cdot \hat{\mathbf{s}}_j + \mathbf{d}_{ij} \cdot (\hat{\mathbf{s}}_i \times \hat{\mathbf{s}}_j)] - \sum_i k(\hat{\mathbf{s}}_i \cdot \hat{\mathbf{z}})^2 - \frac{\mu_0}{8\pi} \sum_{i,j \neq i} \frac{3(\mathbf{S}_i \cdot \mathbf{u}_{ij})(\mathbf{S}_j \cdot \mathbf{u}_{ij}) - \mathbf{S}_i \cdot \mathbf{S}_j}{r_{ij}^3} - \mu_0 \sum_i \mathbf{S}_i \cdot \mathbf{H}, \quad (1)$$

where $\hat{\mathbf{s}}_i = \mathbf{S}_i / \|\mathbf{S}_i\|$. The first two terms are, respectively, the Heisenberg and Dzyaloshinskii-Moriya interaction with respective constants J and \mathbf{d} . Summation is performed on the first-neighbor pairs (i, j) , which accurately describes

^{*}stanislas.rohart@u-psud.fr

Co/Pt(111) [28]. For a thin film, $\mathbf{d}_{ij} = d(\hat{\mathbf{u}}_{ij} \times \hat{\mathbf{z}})$ [2,29], with $\hat{\mathbf{u}}_{ij}$ the unit vector between sites i and j and $\hat{\mathbf{z}}$ the normal to the plane. The third term is the uniaxial anisotropy, with constant k , the fourth term is the dipolar coupling (r_{ij} is the distance between sites i and j), and the last term is the Zeeman energy in field \mathbf{H} , applied along $\hat{\mathbf{z}}$ in this study. The parameters are $\mu_{\text{at}} = \|\mathbf{S}_i\| = 2.1\mu_B/\text{atom}$ [30–33], $J = 29$ meV/bond [30], $d = -1.5$ meV/bond [25–27], and $k = 0.4$ meV/atom [31,33] (including the shape anisotropy [34], the effective anisotropy is 0.276 meV/atom, in good agreement with literature [31,33]). The sample is limited by free boundary conditions and the size has been chosen so that an isolated skyrmion is not affected by the edges (no morphology or energy changes are seen for larger calculation box sizes).

The ground state of our system is ferromagnetic, which means that DMI is not sufficient to destabilize the collinear magnetic order, in agreement with experimental observations (the onset of ferromagnetic order instability is $d_c = 2.08$ meV here). The ferromagnetic order remains stable for all temperatures up to the Curie temperature, estimated to be 375 K (using Monte Carlo simulations—not shown). However, when a skyrmion is introduced, it remains as a metastable state. The skyrmion [see Fig. 1(a)] has a radial symmetry with a hedgehog configuration (in-plane magnetization pointing along the radial

direction). Conceivably, skyrmions could be centered on a lattice site or have their core split up over a lattice triangle. The latter structure is found to have the smallest energy, although the energy difference proves to be minute. For the present parameters and in zero field, its energy is 485 meV, with a diameter of 4.6 nm, in quite good agreement with analytical predictions [9].

III. SKYRMION COLLAPSE PATH

Deciphering the collapse mechanism implies a search for the easiest path that links the skyrmion to ferromagnetic state. This has been achieved, although not at the atomic scale, in the case of magnetic vortex core reversal [18]—a problem quite close to ours—and good agreement with the thermal fluctuation method was reached [35]. To determine the minimum energy path between two stable configurations on the multidimensional energy surface [36], 21 images, from the skyrmion to the uniform state, are energy minimized simultaneously. Relaxation occurs in the plane orthogonal to the tangent between successive images [37]. An elastic force along the tangent is also added to ensure equidistance between the images, relying on a geodesic metric [23,37]. Given the complexity of the energy surface and the large number of degrees of freedom, several stable paths may be obtained depending on the initial guess.

Two paths have been identified (see Fig. 1). Path 1 is characterized by a progressive skyrmion diameter reduction down to zero [Figs. 1(b) and 1(c)], the texture being almost self-similar along the path. Such a path may appear as natural and is the only one considered in previous studies [20,23]. Path 2 appears more sophisticated, involving, on top of an overall skyrmion diameter reduction as in path 1, a large rotation of the center spins in the radial direction and in a sense opposing the DMI favored chirality, which can be viewed as a coherent excitation of the most central spins [Figs. 1(b) and 1(d)]. For path 1 the energy increase is progressive and the maximum (saddle point) is reached when the skyrmion is compressed down to the few last center lattice sites [Fig. 1(b)]. For path 2, the initial energy rise proves faster, but the saddle point is obtained much earlier, showing that the rotation of the center spins efficiently contributes to the skyrmion destabilization [Fig. 1(b)]. Path 2 proves to be the lowest energy one with an energy barrier of 64 meV compared to 90 meV for path 1. Under a finite (destabilizing, i.e., oriented opposite to the skyrmion core) field of 250 mT, path 2 is also found to be the easiest one with an energy barrier falling to 30 meV. Path 2 also exhibits a larger susceptibility to field as compared to path 1 [Fig. 1(b)].

These static results are compared to thermally induced collapse using Langevin dynamics. Although this method hardly allows for a description of the collapse mechanism, it is free from any hypothesis on the collapse path. It involves a large amount of calculations to account for the process statistics, so that the time scale that can be reasonably explored is only a few tens of nanoseconds. In order to observe a significant number of skyrmion collapse events, stability is only considered under a 250 mT out-of-plane destabilizing field and calculations have been conducted around 80 K, with no less than 100 collapse events per temperature.

As a first outcome of these calculations, skyrmion diffusion is observed [Fig. 2(a)]: The skyrmion being a soliton and

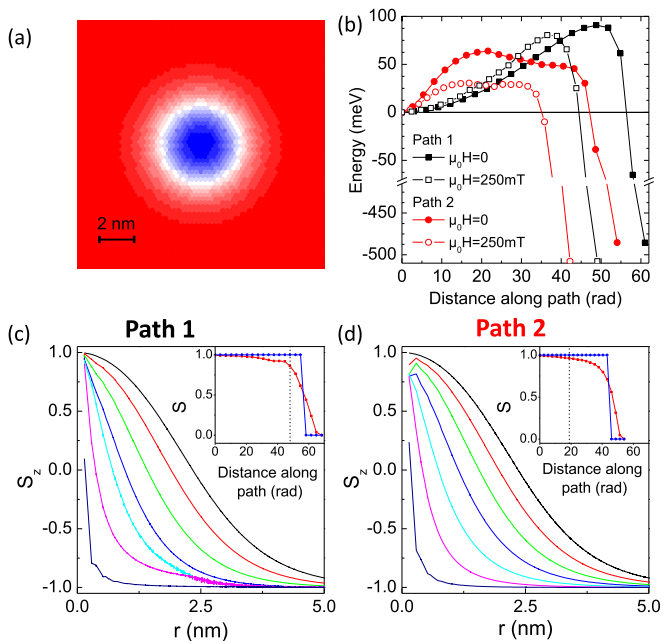


FIG. 1. (a) Skyrmion configuration in zero field. The color code represents the perpendicular spin component from blue (upward) to red (downward) through white (in plane). (b) Energy variation along the collapse path. The distance along the path corresponds to the geodesic metric [23,37]. (c), (d) Variation of the perpendicular spin component as a function of the radial distance for successive configurations along the collapse path (starting from the skyrmion state, the profiles are plotted for every third configuration along the path) in zero magnetic field. In (c) the path only involves diameter reduction (path 1). In (d) the path involves both skyrmion diameter reduction and skyrmion center spin rotation (path 2). In the insets, the variations of the skyrmion number with two definitions (see text) are plotted (the dotted line indicates the position of the energy maximum).

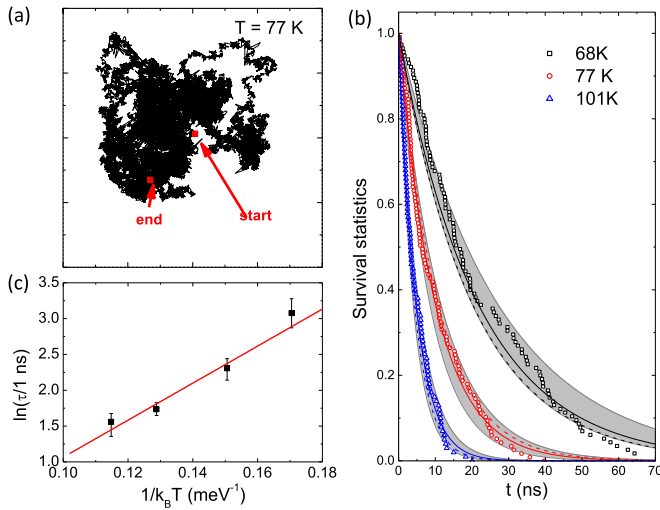


FIG. 2. (a) Trajectory of a skyrmion submitted to thermal noise at 77 K, from start (initial position) to end (skyrmion collapse). The frame represents the 200×200 nm 2 calculation box. Skyrmion collapse occurs here after 28 ns. (b) Survival statistics vs time for three different temperatures. The solid line is the $\exp(-t/\tau)$ model (with τ the mean collapse time, function of temperature) and the gray shaded area represents the uncertainty on τ . (c) Arrhenius plot of the mean lifetime τ vs temperature. The line is a fit to the data leading to activation energy and attempt time.

its energy independent of position, a free random walk is indeed expected [38,39]. After some time, the skyrmion vanishes suddenly. The survival statistics obtained from the collapse time distributions [Fig. 2(b)] is well fitted by a simple exponential decay for all four temperatures considered, suggesting that only one Markovian process is involved. Of course, the higher the temperature, the shorter the mean lifetime τ . An activation energy is extracted [22,24] from the Arrhenius law $\tau = \tau_0 \exp(\Delta E/k_B T)$. In our case, although the agreement is not perfect, indicating that such a law may be oversimplified (for example, no temperature dependence of τ_0 is included), it sets the order of magnitude of the energy barrier to $\Delta E = 26 \pm 4$ meV and $\tau_0 = 0.22 \pm 0.1$ ns [Fig. 2(c)], in good agreement with the lowest energy barrier found using the path analysis.

IV. DISCUSSION

A. Role of topology

In order to assess the role of topology in the skyrmion stability, a topological number S along the path needs to be defined. In the original work of Feldtkeller that deals with continuous textures [15], two equivalent definitions are given. The *geometrical* definition measures the proportion of the unit sphere (the order parameter space) covered by the spin texture projected onto it. This quantity is *mathematically* expressed as $S = (4\pi)^{-1} \int \mathbf{m} \cdot (\partial \mathbf{m} / \partial x \times \partial \mathbf{m} / \partial y) dx dy$. Both definitions can be extended to a discrete set of spins, either (geometrical S) by tiling the unit sphere with oriented spherical triangles whose apices coincide with the projections of neighboring spins on the same unit sphere [18], or (finite differences S) by substituting discrete to ordinary partial derivatives in the

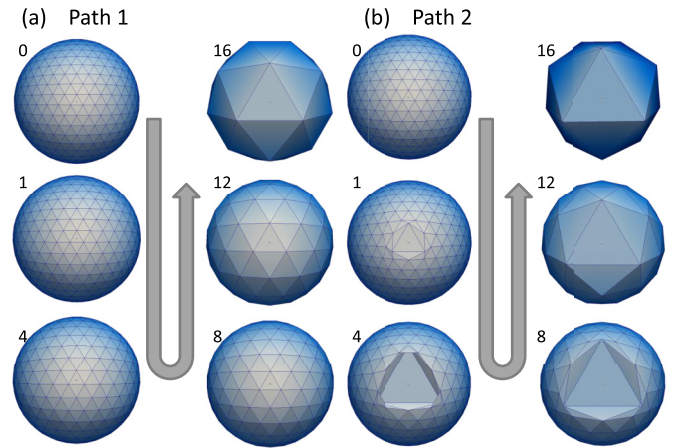


FIG. 3. (a) Mapping on the unit sphere, viewed from well above the top hemisphere (skyrmion core orientation), of six magnetic textures belonging to path 1 for $H_a = 0$. Each node on the sphere corresponds to a spin with its origin at the sphere center and its end point at the node. The drawn net is made out of straight lines (in 3D space) connecting points corresponding to nearest neighbors. Numbers refer to the various images along the path, starting with 0, corresponding to the skyrmion at equilibrium, ending with 20, corresponding to the uniform state. Image 16 corresponds to the maximum energy. Path 1 is characterized by an homogeneous opening up of the spin distribution that matches a gradual shrinking of the skyrmion radius in the physical space. The color scale represents reflectivity towards the observer, for a light source that is vertically situated with a small tilt towards the top of the page. (b) Same as (a) for path 2. Here, the energy maximum occurs at image 8. Together with a gradual opening of the spin distribution, path 2 is primarily characterized by a strong fanning out of the three core spins. Note that, from image 2 onwards, some nearest-neighbor links are hidden, and triangles are significantly inclined with respect to the local sphere tangential plane.

expression of S [37]. These two definitions, however, no longer prove to be equivalent: Whereas the geometrical description still yields integer S values, the finite difference formulation leads to various values and thus may describe a continuous transition from the skyrmion to the ferromagnetic state. In Figs. 1(c) and 1(d), the variation of S along the path is shown for both definitions.

Mapping the spins on the unit sphere (order parameter space) provides a simple and efficient representation of the texture topology along a path. In Fig. 3, only the top hemisphere is visible (along the skyrmion core orientation). In the skyrmion state, the regular tiling of the sphere underlines a smooth texture for the few-nanometer-diameter skyrmion. Along path 1 [Fig. 3(a)], the gradual swelling of the triangular spin lattice pattern simply represents the regular skyrmion shrinking process. In image 16, which corresponds to the energy maximum, only a few spins still have a component along the top pole direction. The onset of path 2 is markedly different [Fig. 3(b)]. From the very beginning, a very local, and symmetrical, distortion of the three most inner spins is allowed for. The distortion grows with image number, retaining the threefold symmetry. In image 8, which corresponds to the energy maximum, the number of spins with a component

along the top hemisphere direction is already strongly reduced, although it is still larger than the number of spins with the same property in image 16 of path 1. Adding a moderate skyrmion destabilizing uniform field only marginally modifies these patterns. The topology change occurs when the top hemisphere is fully depleted, and when three spins (those at the center) lie on the equator, thus in plane, pointing radially. This last configuration is similar, in two dimensions (2D), to the horizontal cut through the Bloch point observed in thicker samples [18]. The maximum in energy is thus obtained before (or even well before in path 2) the topological transition [37]. A trivial analogy is to consider the magnetization textures as elastic nets through which one tries to extract a balloon. Path 1 strains the whole net whereas path 2 concentrates the strain on a single mesh cell.

B. Energy considerations

We now investigate the contribution of the different energy terms to the barrier, as shown for every energy component along paths 1 and 2 in Fig. 4, both for $H_a = 0$ and $\mu_0 H_a = -0.25$ T. The variations of the dipolar coupling and anisotropy, although opposite in sign, are equivalent, which indicates that dipolar coupling mainly acts as a shape anisotropy (0.124 meV/atom) and that the sum of both of them can be considered as an effective anisotropy. A common feature to all graphs is the large relative variation along the path of the (effective) anisotropy and Dzyaloshinskii-Moriya energies as

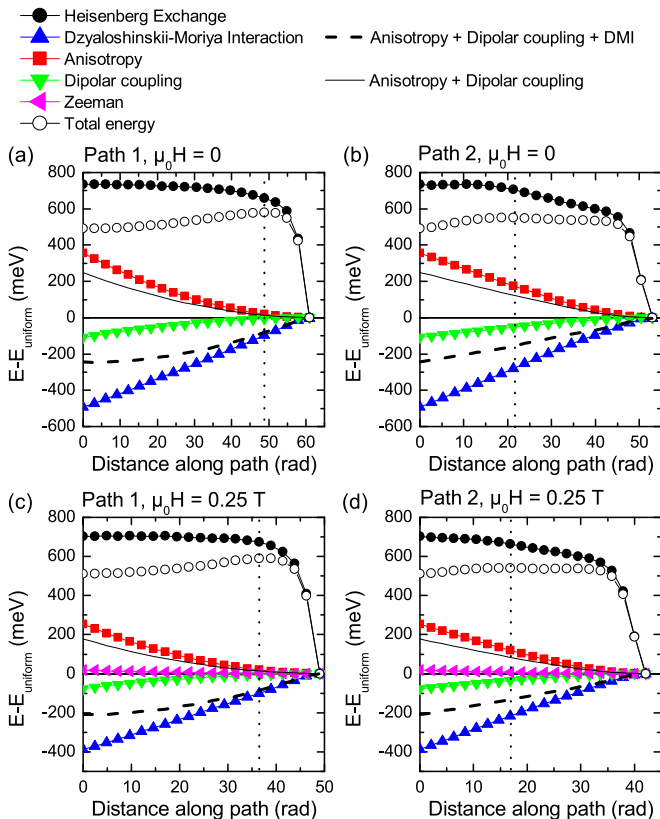


FIG. 4. Variation of the various energy contributions along paths 1 and 2 and at 0 and 0.25 T. The vertical dotted lines indicate the position of the total energy maximum (energy barrier).

compared to the exchange or Zeeman energies. It even appears that, in the approach to the maximum energy along a given path, the slope of the total energy is governed by the behavior of the sum of the effective anisotropy and Dzyaloshinskii-Moriya energies. Note in this respect that this sum monotonously increases towards the barrier top for path 2, whereas it first goes through a minimum for path 1. In contradistinction, the exchange energy is almost constant in this part of the path (see the Appendix).

V. INCREASING SKYRMION LIFETIME

From these results, it is possible to estimate the lifetime of an isolated skyrmion in zero magnetic field, using $\tau_0 = 0.22$ ns and $\Delta E = 64$ meV (note that the error bar on τ_0 is not taken into account as it does not change the order of magnitude of the lifetime). It implies that whereas it is almost infinite at 4 K, the lifetime is only 4 μ s at 77 K and 3 ns at room temperature. Whereas zero-temperature calculations do show for material parameters, such as those discussed above, the possibility to stabilize isolated skyrmions, the latter can only be studied at really low temperatures to avoid thermal collapse.

The poor stability observed here is due to the monolayer thickness on the one hand, but also, on the other hand, to too low a DMI. Indeed, whereas a moderate DMI is required to avoid a spontaneous skyrmion lattice, the DMI value used here is only 72% of the maximum possible value allowing for isolated skyrmions. To study the influence of the DMI on skyrmion stability, we have arbitrarily varied its magnitude d . Previous methods could not be used for calculation time reasons so that we need to introduce an *ad hoc* method. Having identified the crucial role of the spins at the skyrmion center, we manipulate them by imposing their orientation, thus mimicking the lowest energy path, and then obtain the spin configuration at equilibrium for the other sites via energy minimization. The validity of this approach compared to the path method is checked by verifying that, for the center spins, due to the symmetry, the effective field is aligned with the tangent between successive images. By varying the center angle from 0° (skyrmion state) to 180° (uniform state), the results prove quite close to the easiest path found previously [Fig. 5(a)], but with a much reduced calculation time. We observe that the reaction to a small change of the center spin

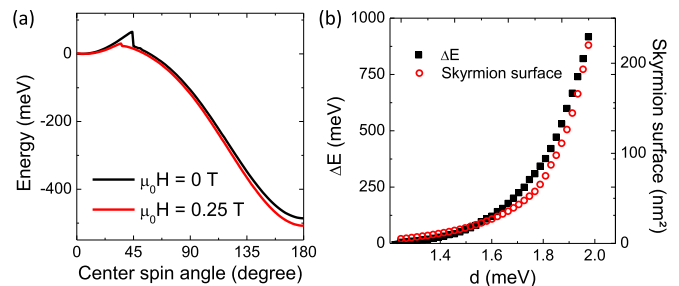


FIG. 5. (a) Skyrmion energy variation as a function of an imposed spin angle for the center spins for 0 and 0.25 T fields. The energy reference is the skyrmion energy. (b) Collapse activation energy and skyrmion surface as a function of the DMI strength calculated using the same method as in (a).

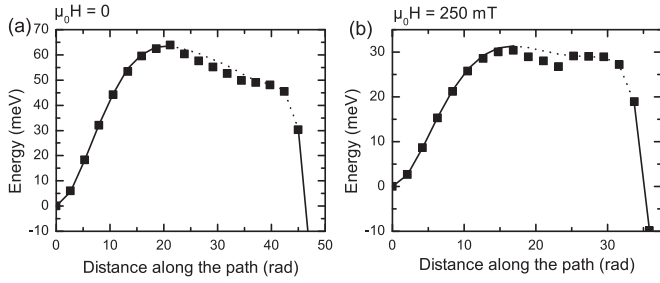


FIG. 6. Energy variations along the collapse path for the *ad hoc* method (lines) and the path method for path 2 (square dots) in (a) 0 and (b) 250 mT fields and for $d = 1.5$ meV. The solid line indicates energies for configurations that are stable for the imposed center spin angle. The dotted line corresponds to the energy drop that occurs in the calculation [see Fig. 3(a)] above a certain imposed center spin angle, and thus to configurations that are not stable with respect to the imposed angle.

tilt is a skyrmion diameter reduction and an energy increase. Above a critical tilt angle, the configuration undergoes a brutal change synonymous with a skyrmion collapse (the noncollinear situation remaining only in the vicinity of the center spins) and an energy drop. A further increase of the tilt angle describes a progressive transition to the ferromagnetic state. Both before and after the critical angle, the energy curve versus metrics is almost undistinguishable from the more rigorous path method calculation (the maximum energy is overestimated by about 3%). The brutal configuration change corresponds to a large jump along the path (see Fig. 6). The variation of the collapse activation energy as a function of d , shown in Fig. 5(b), displays a strong nonlinear dependence. It appears that a modest increase of DMI significantly improves the stability. As an example, an increase of 0.2 meV ($\approx 13\%$) results in $\Delta E = 220$ meV (240% increase). In that case the skyrmion lifetime becomes 13 h at 77 K and 1 μ s at room temperature. Such a dependence can be interpreted by an increase of the skyrmion diameter (for $d = 1.7$ meV, the diameter increases to 7.3 nm), which increases the amount of spins to be reversed. However, the correlation between ΔE and the skyrmion surface is not exact as the energy barrier results from a complex balance of energies, and as also presumed because the isolated skyrmion size diverges at the critical DMI value.

VI. CONCLUSION

In conclusion, we have studied the collapse of isolated skyrmions and identified a nontrivial easiest mechanism as a progressive diameter reduction combined with a rotation of spins at the skyrmion center. For such a mechanism, the destabilization occurs much before any topology change, suggesting that topology plays a minor role, with respect to the micromagnetic energy balance. On the contrary, the DMI energy is shown to play an important role. Despite

the rather poor skyrmion stability found in the monolayer Co/Pt(111), our study opens a route to improve it. A modest DMI increase, using interface engineering combining under and top layers with opposite sign DMI, as a Pt/Co/Ir [26,40] or Pt/Co/MgO [41], could be a solution toward room-temperature stability for nanometer sized skyrmions.

ACKNOWLEDGMENTS

This work was supported by Agence Nationale de la Recherche under Contract No. ANR-14-CE26-0012 ULTRA-SKY. We thank members of this consortium, especially A. Fert and J. Sampaio, for stimulating discussions.

APPENDIX

The near constancy of the exchange energy can be understood simply. On the one hand, in the continuous formulation we immediately see that the exchange energy is invariant under spatial expansion [$\mathbf{m}(x, y) \rightarrow \mathbf{m}(\lambda x, \lambda y)$]. On the other hand, in the discrete formulation, the energy cost of nonparallel nearest-neighbor spins is

$$E_{\text{exc},ij} = J(1 - \hat{\mathbf{s}}_i \cdot \hat{\mathbf{s}}_j) = J(1 - \cos \theta_{ij}). \quad (\text{A1})$$

The last formula has a geometrical interpretation: The area on the unit sphere of the cone C_{ij} of axis $\hat{\mathbf{s}}_i$ and with $\hat{\mathbf{s}}_j$ on its generatrix is

$$C_{ij} = 2\pi(1 - \cos \theta_{ij}). \quad (\text{A2})$$

If the distribution of the spins on the unit sphere is regular, one then expects that

$$C_{ij} \approx 3(T_{ij}^+ + T_{ij}^-), \quad (\text{A3})$$

where T_{ij}^\pm are the two spherical triangles that have $\hat{\mathbf{s}}_i$ and $\hat{\mathbf{s}}_j$ as apices. Instead of the approximate equality, we can introduce a numerical factor f , whose value is $2\pi/(3\sqrt{3})$ for infinitely small triangles. By summation over the bonds one gets

$$E_{\text{exc}} = \sum_{(i,j)} E_{\text{exc},ij} = \frac{9fJ}{2\pi} \sum T. \quad (\text{A4})$$

If the sphere is covered once, then $\sum T = 4\pi$, so that a constant exchange energy is found, with a value

$$E_{\text{exc}} = 18fJ = 4\pi\sqrt{3}J, \quad (\text{A5})$$

the latter equality stemming from using the value of f for regular small triangles. Numerically, with $J = 29$ meV, one finds $E_{\text{exc}} = 631$ meV, of the same order as the numerical results. The (cumbersome) expression of f for finite size equilateral spherical triangles shows that it decreases as the triangle size increases, hence the observed decrease of the exchange energy along the path. This result is in contrast with that of the continuous approach, where it was proved [42] that $E_{\text{exc}} \geq 8\pi A_{2D}$, with $A_{2D} = J\sqrt{3}/2$ the micromagnetic exchange constant for the corresponding 2D medium.

[1] I. E. Dzyaloshinskii, Sov. Phys. JETP **20**, 665 (1965).

[2] T. Moriya, Phys. Rev. **120**, 91 (1960).

[3] A. Yoshimori, J. Phys. Soc. Jpn. **14**, 807 (1959).

[4] J. Villain, J. Phys. Chem. Solids **11**, 303 (1959).

- [5] A. N. Bogdanov and U. K. Röbber, *Phys. Rev. Lett.* **87**, 037203 (2001).
- [6] X. Z. Yu, Y. Onose, N. Kanazawa, J. H. Park, J. H. Han, Y. Matsui, N. Nagaosa, and Y. Tokura, *Nature (London)* **465**, 901 (2010).
- [7] S. Heinze, K. von Bergmann, M. Menzel, J. Brede, A. Kubetzka, R. Wiesendanger, G. Bihlmayer, and S. Blügel, *Nat. Phys.* **7**, 713 (2011).
- [8] N. S. Kiselev, A. N. Bogdanov, R. Schäfer, and U. K. Röbber, *Phys. Rev. Lett.* **107**, 179701 (2011).
- [9] S. Rohart and A. Thiaville, *Phys. Rev. B* **88**, 184422 (2013).
- [10] A. Fert, V. Cros, and J. Sampaio, *Nat. Nanotechnol.* **8**, 152 (2013).
- [11] X. Zhang, M. Ezawa, and Y. Zhou, *Sci. Rep.* **5**, 9400 (2015).
- [12] N. Romming, C. Hanneken, M. Menzel, J. Bickel, B. Wolter, K. von Bergmann, A. Kubetzka, and R. Wiesendanger, *Science* **341**, 636 (2013).
- [13] W. Jiang, P. Upadhyaya, W. Zhang, G. Yu, M. Jungfleisch, F. Fradin, J. E. Pearson, Y. Tserkovnyak, K. L. Wang, O. Heinonen *et al.*, *Science* **349**, 283 (2015).
- [14] S. Woo, K. Litzius, B. Krüger, M.-Y. Im, L. Caretta, K. Richter, M. Mann, A. Krone, R. M. Reeve, M. Weigand *et al.*, *Nat. Mater.* **15**, 501 (2016).
- [15] E. Feldtkeller, *Z. Angew. Phys.* **19**, 530 (1965).
- [16] A. P. Malozemoff and J. C. Slonczewski, *Magnetic Domain Walls in Bubble Materials* (Academic, New York, 1979).
- [17] T. Shinjo, T. Okuno, R. Hassdorf, K. Shigeto, and T. Ono, *Science* **289**, 930 (2000).
- [18] A. Thiaville, J. M. García, R. Dittrich, J. Miltat, and T. Schrefl, *Phys. Rev. B* **67**, 094410 (2003).
- [19] J. Sampaio, V. Cros, S. Rohart, A. Thiaville, and A. Fert, *Nat. Nanotechnol.* **8**, 839 (2013).
- [20] A. D. Verga, *Phys. Rev. B* **90**, 174428 (2014).
- [21] Y. Zhou, E. Iacocca, A. A. Awad, R. K. Dumas, F. C. Zhang, H. B. Braun, and J. Åkerman, *Nat. Commun.* **6**, 8193 (2015).
- [22] J. Hagemester, N. Romming, K. von Bergmann, E. Y. Vedmedenko, and R. Wiesendanger, *Nat. Commun.* **6**, 8455 (2015).
- [23] P. Bessarab, V. M. Uzdin, and H. Jónsson, *Comput. Phys. Commun.* **196**, 335 (2015).
- [24] L. Rózsa, E. Simon, K. Palotás, L. Udvardi, and L. Szunyogh, *Phys. Rev. B* **93**, 024417 (2016).
- [25] F. Freimuth, S. Blügel, and Y. Mokrousov, *J. Phys.: Condens. Matter* **26**, 104202 (2014).
- [26] H. Yang, A. Thiaville, S. Rohart, A. Fert, and M. Chshiev, *Phys. Rev. Lett.* **115**, 267210 (2015).
- [27] M. Belmeguenai, J.-P. Adam, Y. Roussigné, S. Eimer, T. Devolder, J.-V. Kim, S. M. Cherif, A. Stashkevich, and A. Thiaville, *Phys. Rev. B* **91**, 180405 (2015).
- [28] B. Dupé, M. Hoffmann, C. Paillard, and S. Heinze, *Nat. Commun.* **5**, 4030 (2014).
- [29] A. Fert, *Mater. Sci. Forum* **59-60**, 439 (1990).
- [30] O. Šipr, S. Bornemann, J. Minár, S. Polesya, V. Popescu, A. Simunek, and H. Ebert, *J. Phys.: Condens. Matter* **19**, 096203 (2007).
- [31] P. Gambardella, S. Rusponi, M. Veronese, S. S. Dhesi, C. Grazioli, A. Dallmeyer, I. Cabria, R. Zeller, P. H. Dederichs, K. Kern *et al.*, *Science* **300**, 1130 (2003).
- [32] N. Nakajima, T. Koide, T. Shidara, H. Miyauchi, H. Fukutani, A. Fujimori, K. Iio, T. Katayama, M. Nývlt, and Y. Suzuki, *Phys. Rev. Lett.* **81**, 5229 (1998).
- [33] G. Moulas, A. Lehnert, S. Rusponi, J. Zabloudil, C. Etz, S. Ouazi, M. Etzkorn, P. Bencok, P. Gambardella, P. Weinberger *et al.*, *Phys. Rev. B* **78**, 214424 (2008).
- [34] S. Rohart, V. Repain, A. Thiaville, and S. Rousset, *Phys. Rev. B* **76**, 104401 (2007).
- [35] R. Dittrich, T. Schrefl, A. Thiaville, J. Miltat, V. Tsiantos, and J. Fidler, *J. Magn. Magn. Mater.* **272-276**, 747 (2004).
- [36] G. Henkelman and H. Jónsson, *J. Chem. Phys.* **113**, 9978 (2000).
- [37] See Supplemental Material at <http://link.aps.org/supplemental/10.1103/PhysRevB.93.214412> for additional information about the path minimization procedure and the definition of the topological number for a discrete system.
- [38] A. Einstein, *Ann. Phys.* **17**, 459 (1905).
- [39] C. Schütte, J. Iwasaki, A. Rosch, and N. Nagaosa, *Phys. Rev. B* **90**, 174434 (2014).
- [40] A. Hrabec, N. A. Porter, A. Wells, M. J. Benitez, G. Burnell, S. McVitie, D. McGrouther, T. A. Moore, and C. H. Marrows, *Phys. Rev. B* **90**, 020402 (2014).
- [41] O. Boule, J. Vogel, H. Yang, S. Pizzini, D. de Souza Chaves, A. Locatelli, T. O. Mendes, A. Sala, L. D. Buda-Prejbeanu, O. Klein *et al.*, *Nat. Nanotechnol.* **11**, 449 (2016).
- [42] A. A. Belavin and A. M. Polyakov, *JETP Lett.* **22**, 245 (1975).